*8th International Conference on Contact Mechanics and Wear of Rail/Wheel Systems (CM2009), Firenze, Italy, September 15-18, 2009*

# AN INNOVATIVE WHEEL - RAIL CONTACT MODEL FOR MULTIBODY APPLICATIONS

**Silvia Magheri*, Monica Malvezzi*, Enrico Meli*, Andrea Rindi***

* University of Florence, Department of Energy Engineering S. Stecco
Via S. Marta 3, 50139, Firenze, ITALIA
silvia.magheri@unifi.it, malvezzi@mapp1.de.unifi.it,
meli@mapp1.de.unifi.it, rindi@mapp1.de.unifi.it

## ABSTRACT

The wheel – rail contact analysis plays a fundamental role in the multibody modeling of railway vehicles. A good contact model must provide an accurate description of the global and local contact phenomena (contact forces, position and shape of the contact patch, stress and strain) and a general handling of the multiple contact. The model has also to assure high numerical efficiency and a good compatibility with commercial multibody software (Simpack, Adams).
In this work the authors intend to present an innovative elastic wheel – rail contact model that satisfies the previous specifics. The model considers the wheel and the rail as elastic deformable bodies and requires the numerical solution of the Navier's elasticity equation. The contact between wheel and rail has been described by means of suitable analytical contact conditions. Subsequently the contact model has been inserted within the multibody model of a benchmark railway vehicle (the Manchester Wagon) in order to obtain a complete model of the wagon. The whole model has been implemented in the Matlab/Simulink environment. Finally numerical simulations of the vehicle dynamics have been carried out on many different railway tracks with the aim of evaluating the performance of the model.
The multibody model of the same vehicle (this time equipped with a standard contact model) has been then implemented also in Simpack Rail. The comparison between the results obtained by the Matlab model and those obtained by the Simpack model has allowed an accurate and reliable validation of the new contact model.
In conclusion the main purpose of the authors is to achieve a better integration between the differential modeling and the multibody modeling. This kind of integration is almost absent in literature (especially in the railway field) due to the computational cost and to the memory consumption. However it is very important because only the differential modeling allows an accurate analysis of the contact problem (in terms of contact forces, position and shape of the contact patch, stress and strain) while the multibody modeling is currently the standard in the study of the railway dynamics.

## 1 INTRODUCTION

The multibody simulation of the railway vehicle dynamics needs a reliable contact model that satisfies the following specifics: accurate description of the global and local contact phenomena (contact forces, position and shape of the contact patch, stress and strain), general and robust handling of the multiple contact, high numerical efficiency and compatibility with commercial multibody software (Simpack Rail, Adams Rail).
The wheel – rail contact problem has been discussed by several authors and many models can be found in the literature. All the contact model specifically designed for the multibody modeling (as the so-called rigid contact formulation [1]-[6] and the semi-elastic contact description [4]-[8]) are computationally very efficient but their generality and accuracy turn out to be often insufficient. In particular, the physical theories behind this kind of models (Hertz's and Kalker's theory) require very restrictive hypotheses that, in many circumstances, are unverified.
Differential contact models are needed if a detail description of the contact phenomena is required. In other words wheel and rail have to be considered elastic bodies governed by the Navier's equations and the contact has to be described by suitable analytical contact conditions. This kind of approach assures high generality and accuracy but still needs very large computational costs and memory consumption [4] [9]-[13]. For this reason, the integration between multibody and differential modeling is almost absent in literature especially in the railway field. However this integration is very important because only the differential modeling allows an accurate analysis of the contact problem while the multibody modeling is the standard in the study of the railway dynamics.
In this work the authors intend to present an innovative differential contact model with the aim of achieving a better integration between multibody and differential modeling. The new contact model is fully 3D and satisfies all the specifics described above. The developed procedure requires the discretization of the elastic contact problem (Navier's equations and analytical contact condition) and subsequently the solution of the nonlinear discrete problem. Both the steps have been implemented in Matlab/Simulink environment.
At this point the contact model has been inserted within a 2D multibody model of a railway vehicle to obtain a complete model of the wagon. The railway vehicle chosen as benchmark is the Manchester Wagon [14]. The choice of a 2D multibody model allows to study the lateral vehicle dynamics and at the same time to

reduce the computational load. In the near future fully 3D multibody models will be considered in order to have a complete description of the vehicle dynamics. The multibody model has been implemented in SimMechanics, a Matlab toolbox specifically designed for multibody dynamics.
The 2D multibody model of the same vehicle (this time equipped with a standard contact model based on the semi – elastic approach) has been then implemented also in Simpack Rail, a commercial multibody software for railway vehicles widely tested and validated.
Finally numerical simulations of the vehicle dynamics have been carried out on many different railway tracks with the aim of evaluating the performance of the whole model. The comparison between the results obtained by the Matlab model and those obtained by the Simpack Rail model has allowed an accurate and reliable validation of the new contact model.

## 2 ARCHITECTURE OF THE MODEL

As said in the introduction the whole model consists of two different part: the 2D multibody model of the railway vehicle and the fully 3D differential wheel – rail contact model. The 2D model has been obtained from a fully 3D multibody model of the benchmark vehicle (the Manchester Wagon, Fig. (1)).

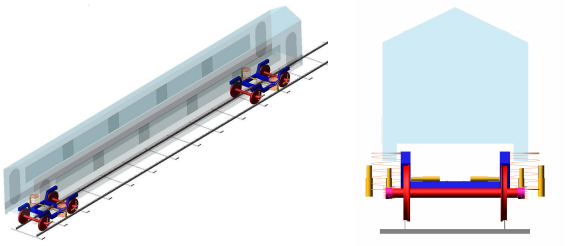

Figure 1: 3D and 2D multibody models of the Manchester Wagon.

The 2D model consists of three bodies: a car – body, a bogie and a wheelset. The car - body and the bogie have 3 DOF (lateral and vertical displacement and roll) while the wheelset has 4 DOF (lateral and vertical displacement, roll and pitch, i.e. the rotation around its symmetry axis). In other words the wheelset has been considered as a 3D body.
During the simulation the 2D multibody model interacts with the fully 3D differential contact model. The general architecture of the model is schematically shown in Fig. (2).

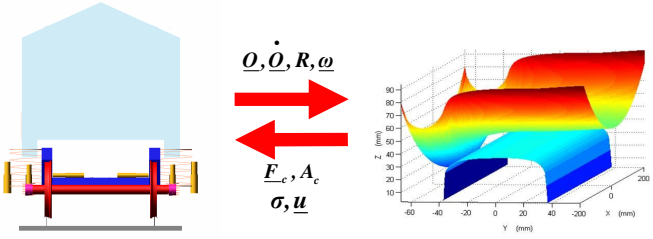


Figure 2: General architecture of the model.

At each integration step the multibody model evaluates the kinematic variables relative to the wheelset and consequently to each wheel – rail pair. Starting from these quantities, the contact model calculates the global and local contact variables (force, contact patch, stress and displacement). Finally the knowledge of the contact variables allows the multibody model to carry on the simulation of the vehicle dynamics.

## 3 REFERENCE SYSTEMS

The railway track can be considered as a 3D curve $\underline{\gamma}(s)$ expressed in a fixed reference system $O_f x_f y_f z_f$ (where $s$ is the curvilinear abscissa of $\underline{\gamma}$). Usually in the cartographic description of the track only the curvature $K(s)$ of $\underline{\gamma}(s)$ and the track slope $p(s)$ are known; however the knowledge of these parameters is enough to rebuild the curve $\underline{\gamma}(s)$. [8] [15]

In this work the lateral vehicle dynamics will be described in a local reference system $O_R x_R y_R z_R$ having the $x_R$ axis tangent to the track in the point $O_R = \underline{\gamma}(s)$ and the $z_R$ axis normal to the plane of the rails. In the considered case the time histories of the curvilinear abscissa $s(t)$ and of the origin $O_R = \underline{\gamma}(s(t))$ are supposed to be known (for instance they can be calculated by simulating independently the longitudinal vehicle dynamics).
The local system follows the motion of the whole model along the track so that the centers of mass of the bodies lie always on the plane $y_R z_R$. According to chapter 2, the car – body and the bogie can only translate along $y_R$ and $z_R$ and rotate around $x_R$ while the wheelset can also rotate around its symmetry axis.
Subsequently a third reference system $O_W x_W y_W z_W$ is defined. The origin $O_W$ coincides with the center of mass of the wheelset and the $y_W$ axis with its symmetry axis. This system is fixed to the wheelset except for the rotation around the $y_W$ axis. Finally two reference systems $O_b x_b y_b z_b$ and $O_B x_B y_B z_B$ are introduced, fixed respectively to the bogie and to the car - body. As usual the origins coincide with the centers of mass. The placement of the reference systems is illustrated in Fig. (3).

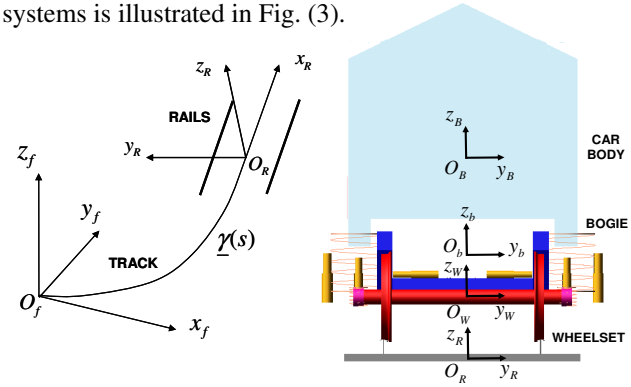


Figure 3: Reference systems relative to the multibody model.

In order to correctly describe the differential contact model, two further reference systems have to be

defined for each wheel – rail pair. For the sake of simplicity only the left pair has been reported in Fig. (4). The first system $O_{lw}x_{lw}y_{lw}z_{lw}$ is parallel to the system $O_W x_W y_W z_W$ and its origin $O_{lw}$ lies on the symmetry axis of the wheel. The system is fixed to the wheel except for the rotation around the $y_{lw}$ axis.

Moreover the origin $O_{lw}$ belongs to the nominal rolling plane, i.e. the plane normal to the rotation axis containing the nominal rolling radius. The second system $O_{lr}x_{lr}y_{lr}z_{lr}$ is parallel to the system $O_R x_R y_R z_R$. Its origin $O_{lr}$ belongs to the axis $y_R$ while the distance between $O_R$ and $O_{lr}$ has to assure the correct gauge between the rails. Both the reference systems described above are very important because the global and local contact variables will be evaluated by the contact model just in these systems.

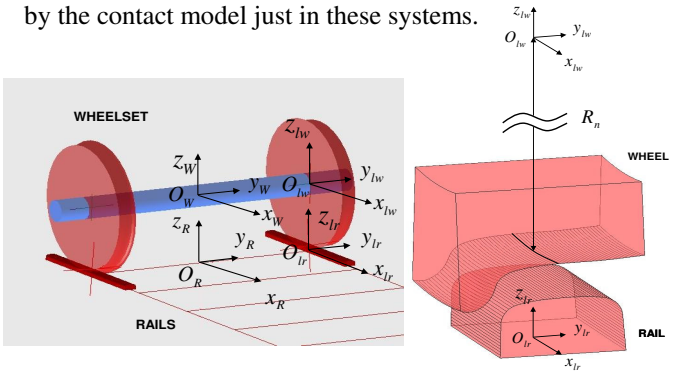


Figure 4: Reference systems relative to the differential contact model.

Finally, as regards the external forces acting on the bodies, some considerations are needed. As said before, the lateral vehicle dynamics is studied in the local reference system $O_R x_R y_R z_R$ but this system is not inertial. Therefore the multibody model will have to consider the effect of the fictitious forces (centrifugal force and Coriolis force). These quantities can be calculated starting from the knowledge of the kinematics of the bodies as a function of the curvature $K(s)$ and of the track slope $p(s)$. [15]

## 4 THE 2D MULTIBODY MODEL

The 2D multibody model has been obtained from a fully 3D multibody model of the Manchester Wagon, the physical and geometrical characteristics of which are easily available in the literature. [14] The original 3D model consists of:
- 1 car – body, 2 bogies and 4 wheelsets
- rear and front primary suspensions
- rear and front secondary suspensions (including roll bar, traction rod and bumpstop).

Both the primary and the secondary suspensions are usually modeled by means of nonlinear force elements like three- dimensional springs and dampers. The 2D model can be thought of as a section of the 3D model and comprises (Fig. (5)):
- one car – body, one bogie and one wheelset
- one primary suspension
- one secondary suspension (including roll bar and bumpstop).

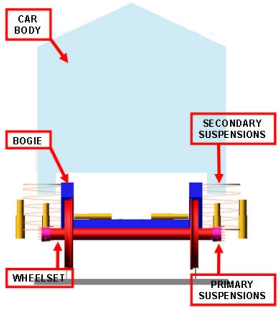


Figure 5: Reference systems relative to the differential contact model.

| Body | Mass | Inertia |
|---|---|---|
| Car – body | 0.25 | 0.25 |
| Bogie | 0.5 | 0.5 |
| Wheelset | 1 | 1 |

Table 1: Scaling factors (mass and inertia).

| Suspensions | Springs | Dampers |
|---|---|---|
| Secondary | 0.5 | 0.5 |
| Primary | 1 | 1 |

Table 2: Scaling factors (springs and dampers).

As regards the bodies, only some DOF are allowed by the 2D model:
- the car – body and the bogie have 3 DOF; they can translate along the axes $y_R$ and $z_R$ (lateral and vertical displacements) and rotate around the $x_R$ axis (roll)
- the wheelset, considered as a 3D body, has 4 DOF; besides the previous DOF it can also rotate around its symmetry axis $y_W$ (pitch).

Moreover, in order to assure the dynamic equivalence between the 2D model and the original 3D model, the inertial characteristics of the bodies and the physical characteristics of the force elements have to be correctly scaled down.[5][14] The values of the scaling factors are schematically reported in Tab. (1) and Tab. (2).
The choice of a 2D multibody model has been made with the aim of studying the lateral vehicle dynamics and, at the same time, of reducing the computational load. In the near future fully 3D multibody models of the Manchester Wagon will be considered in order to have a complete description of the vehicle dynamics.

## 5 THE 3D DIFFERENTIAL CONTACT MODEL

As regards the generic contact variable $Z$, the following convention will be adopted:
- $Z_w$ and $Z_w^r$ will denote a variable relative to the wheel respectively expressed in the reference systems $O_{lw}x_{lw}y_{lw}z_{lw}$ and $O_{lr}x_{lr}y_{lr}z_{lr}$
- $Z_r$ and $Z_r^w$ will denote a variable relative to the rail respectively expressed in the reference systems $O_{lr}x_{lr}y_{lr}z_{lr}$ and $O_{lw}x_{lw}y_{lw}z_{lw}$.

In the future, according to this convention, the various changes of reference system won't be continually remarked but will be taken for granted.

### 5.1 Inputs and Outputs

With reference to Fig. (2), the contact model can be thought of as a black box having the following inputs and outputs:

- INPUTS: the kinematic variables relative to the considered wheel – rail pair (in this case the left one), i.e. the position $\underline{O}_w^r$, the velocity $\dot{\underline{O}}_w^r$, the orientation $R_w^r$ and the angular velocity $\underline{\omega}_w^r$ of the reference system $O_{lw}x_{lw}y_{lw}z_{lw}$ with respect to the system $O_{lr}x_{lr}y_{lr}z_{lr}$ (see Fig. (4)).
- OUTPUTS: the global and local contact variables relative to the wheel and to the rail, like the contact forces $\underline{F}_{wC}$ and $\underline{F}_{rC}$, the stresses $\sigma_w$ and $\sigma_r$, the displacements $\underline{u}_w$ and $\underline{u}_r$ and the contact patches $A_{wC}$ and $A_{rC}$.

### 5.2 The kinematics of the problem

The wheel and the rail have been considered as two linear elastic bodies $\Omega_w$ and $\Omega_r$ (as shown in Fig. (6)). [10][11]

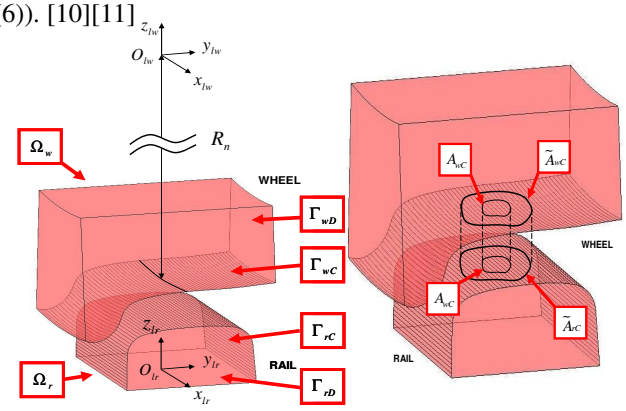


Figure 6: The problem geometry.

Both the domains are supposed to be sufficiently large compared to the dimensions of the contact patch. The boundaries $\partial\Omega_w$ and $\partial\Omega_r$ are split into two disjoint regions, respectively $\Gamma_{wD}$, $\Gamma_{wC}$ and $\Gamma_{rD}$, $\Gamma_{rC}$. Within the regions $\Gamma_{wD}$ and $\Gamma_{rD}$ the displacements are fixed (and equal to zero) while $\Gamma_{wC}$ and $\Gamma_{rC}$ (dashed in the figure) are the regions where the contact may occur. In case of contact the geometric intersection between the surfaces $\Gamma_{wC}$ and $\Gamma_{rC}$ (and thus between the non – deformed configurations) allows to define two regions $\tilde{A}_{wC} \subset \Gamma_{wC}$ and $\tilde{A}_{rC} \subset \Gamma_{rC}$ (with $\tilde{A}_{wC} \simeq \tilde{A}_{rC}$) that can be considered as a rough estimate of the contact areas. The situation is schematically sketched in Fig. (6) and Fig. (7).

The real contact areas $A_{wC} \subset \tilde{A}_{wC}$ and $A_{rC} \subset \tilde{A}_{rC}$ (with $A_{wC} \simeq A_{rC}$) are unknown and have to be calculated by the model. For this purpose a contact map $\underline{\Phi}$ has to be introduced. The contact map $\underline{\Phi} : \tilde{A}_{wC} \to \tilde{A}_{rC}$ (by convention the wheel is the master body) locates the position of the point

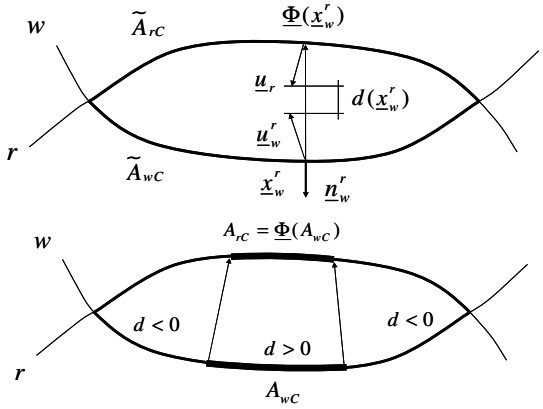


Figure 7: Contact map and distance function.

$\underline{\Phi}(\underline{x}_w^r) \in \tilde{A}_{rC}$ that will come in contact with the generic point $\underline{x}_w^r \in \tilde{A}_{wC}$. In this case the map $\underline{\Phi}$ is defined as the normal projection $\underline{\Phi}(\underline{x}_w^r)$ of the point $\underline{x}_w^r \in \tilde{A}_{wC}$ on the surface $\tilde{A}_{rC}$.

Starting from the contact map, the distance function between the deformed configurations $d : \tilde{A}_{wC} \to R$ can be evaluated:

$$d(\underline{x}_w^r) = \left(\underline{u}_w^r - \underline{u}_r\right) \bullet \underline{n}_w^r - \left(\underline{\Phi}(\underline{x}_w^r) - \underline{x}_w^r\right) \bullet \underline{n}_w^r \qquad (1)$$

where $\underline{n}_w^r$ is the outgoing normal versor to the surfaces $\Gamma_{wC}$. The function $d$ is positive if there is penetration between the deformed configurations and negative otherwise.

Formally the contact area $A_{wC}$ is defined as the region of $\tilde{A}_{wC}$ where the function $d$ is positive while the contact area $A_{rC} = \underline{\Phi}(A_{wC})$ is the normal projection of $A_{wC}$ on $\tilde{A}_{rC}$. In other words, from a kinematic point of view, the penetration between the deformed bodies is allowed and will play a fundamental role in the contact model (see paragraph 5.3). [10][11]

In this way the estimated contact areas $\tilde{A}_{wC}$ and $\tilde{A}_{rC}$ depend only on the relative wheel – rail kinematics ($\underline{O}_w^r$, $\dot{\underline{O}}_w^r$, $R_w^r$ and $\underline{\omega}_w^r$) while the real contact areas $A_{wC}$ and $A_{rC}$ depend also on the displacements $\underline{u}_w$ and $\underline{u}_r$. Finally it is useful to remark that no hypothesis has been made on the shape of the contact patch; in particular, the contact patch can be formed of one or more disjoint parts.

As regards the wheel and rail profiles, the standard ORE S 1002 and UIC 60 have been used. [15]

### 5.3 The contact model

According to the linear theory of elasticity [10] [11], both the wheel and the rail are governed by the Navier's equations:

$$\begin{array}{llll} div\ \sigma_w(\underline{u}_w)=\underline{0} & \text{on } \Omega_w & \sigma_w(\underline{u}_w)\underline{n}_w=\underline{p}_w & \text{on } \widetilde{A}_{wC} \\ div\ \sigma_r(\underline{u}_r)=\underline{0} & \text{on } \Omega_r & \sigma_w(\underline{u}_w)\underline{n}_w=\underline{0} & \text{on } \Gamma_{wC}\setminus\widetilde{A}_{wC} \\ \underline{u}_w=\underline{0} & \text{on } \Gamma_{wD} & \sigma_r(\underline{u}_r)\underline{n}_r=\underline{p}_r & \text{on } \widetilde{A}_{rC} \\ \underline{u}_r=\underline{0} & \text{on } \Gamma_{rD} & \sigma_r(\underline{u}_r)\underline{n}_r=\underline{0} & \text{on } \Gamma_{rC}\setminus\widetilde{A}_{rC} \end{array} \quad (2)$$

where $\underline{n}_w$ and $\underline{n}_r$ are the outgoing normal vectors to the surfaces $\Gamma_{wC}$ and $\Gamma_{rC}$ while $\underline{p}_w$ and $\underline{p}_r$ are the unknown contact pressures. The pressures $\underline{p}_w$ and $\underline{p}_r$ are defined on $\widetilde{A}_{wC}$ and $\widetilde{A}_{rC}$ but, according to paragraph 5.2, will have to be zero on $\widetilde{A}_{wC}\setminus A_{wC}$ and $\widetilde{A}_{rC}\setminus A_{rC}$. Both the bodies have the material characteristics of the steel (Young's modulus $E_w = E_r = 2.1*10^{11}\,Pa$ and Poisson's coefficient $\nu_w = \nu_r = 0.3$). In the studied case the volume forces (i. e. the gravity) have been neglected because the multibody model of the wheelset already considers their effect. Moreover, since the solution is supposed to be steady within the integration step (see Fig. (2)), also the inertial terms have been omitted.

Equivalently the problem (2) can be formulated in weak form as follows:

$$\begin{aligned} \int_{\Omega_w}\sigma_w(\underline{u}_w):\varepsilon_w(\underline{v}_w)dV &= \int_{\widetilde{A}_{wC}}\underline{p}_w\bullet\underline{v}_w dA \quad \forall\underline{v}_w\in V_w \\ \int_{\Omega_r}\sigma_r(\underline{u}_r):\varepsilon_r(\underline{v}_r)dV &= \int_{\widetilde{A}_{rC}}\underline{p}_r\bullet\underline{v}_r dA \quad \forall\underline{v}_r\in V_r \end{aligned} \quad (3)$$

where $\varepsilon_w$ and $\varepsilon_r$ are the strains while $V_w$ and $V_r$ are suitable Sobolev's spaces.

In order to complete the contact model, the contact pressures $\underline{p}_w$ and $\underline{p}_r$ have to be expressed as a function of the displacements $\underline{u}_w$ and $\underline{u}_r$.

For the sake of simplicity the normal and the tangential contact pressures on the wheel are introduced: $p^r_{wN} = \underline{p}^r_w\bullet\underline{n}^r_w$, $\underline{p}^r_{wT} = \underline{p}^r_w - p^r_{wN}\underline{n}^r_w$.

The normal pressure $p^r_{wN}$ has been calculated by means of the distance function $d$:

$$p^r_{wN}(\underline{x}^r_w) = -K\max(d(\underline{x}^r_w),0) \quad \text{on } \widetilde{A}_{wC} \quad (4)$$

where $K>0$ is a fictitious stiffness constant. The value of K have to be chosen large enough to assure the accuracy required by this kind of problems. The condition of ideal contact (total absence of penetration between the deformed bodies) is reached for $K\to+\infty$ (usually $K\geq 10\text{^}15\ \text{N/m}^3$).[10][11]

To evaluate the tangential pressure $\underline{p}^r_{wT}$, the slip $\underline{s}^r_w$ between the wheel and rail surfaces has to be defined. Since the solution is supposed to be steady within the integration step, the following expression holds: [4]

$$\begin{aligned} \dot{\underline{s}}^r_w(\underline{x}^r_w) &= \dot{\underline{w}}^r_w(\underline{x}^r_w) + \dot{\underline{u}}^r_w(\underline{x}^r_w) - \dot{\underline{w}}_r(\Phi(\underline{x}^r_w)) - \dot{\underline{u}}_r(\Phi(\underline{x}^r_w)) = \\ &= \underline{w}^r_w(\underline{x}^r_w) + J^r_w(\underline{x}^r_w)\,\underline{w}^r_w(\underline{x}^r_w) - \underline{w}_r(\Phi(\underline{x}^r_w)) - J_r(\Phi(\underline{x}^r_w))\,\underline{w}_r(\Phi(\underline{x}^r_w)) \end{aligned} \quad (5)$$

where $\underline{w}^r_w$ and $\underline{w}_r$ are the rigid velocity of the points $\underline{x}^r_w$ and $\Phi(\underline{x}^r_w)$ while $J^r_w$ and $J_r$ are the Jacobians of $\underline{u}^r_w$ and $\underline{u}_r$. As usual the normal and the tangential slips are: $s^r_{wN} = \underline{s}^r_w\bullet\underline{n}^r_w$, $\underline{s}^r_{wT} = \underline{s}^r_w - s^r_{wN}\underline{n}^r_w$. According to the standard friction models, the tangential pressures $\underline{p}^r_{wT} = \underline{p}^r_{wT}(\underline{x}^r_w)$ can be expressed as follows:

$$\underline{p}^r_{wT} = \begin{cases} \underline{0} & \text{if } s^r_{wT}=0 \\ -\mu(s^r_{wT},V)\left|p^r_{wN}\right|\dfrac{\underline{s}^r_{wT}}{s^r_{wT}} & \text{if } s^r_{wT}>0 \end{cases} \quad \text{on } \widetilde{A}_{wC} \quad (6)$$

where $s^r_{wT}$ is the norm of $\underline{s}^r_{wT} = \underline{s}^r_{wT}(\underline{x}^r_w)$ and $V$ is the longitudinal velocity of the vehicle. Further details on the friction function $\mu(s^r_{wT},V)$ can be found in the literature. [17]

Finally the action – reaction principle (the Newton's Third Law) allows to calculate the pressures $\underline{p}_r$:

$$\underline{p}_r(\Phi(\underline{x}^r_w)) = -\underline{p}^r_w(\underline{x}^r_w) \quad \text{on } \widetilde{A}_{wC}. \quad (7)$$

It is useful to remark that, according to the described model, the pressures $\underline{p}^r_w$ and $\underline{p}_r$ are zero respectively on $\widetilde{A}_{wC}\setminus A_{wC}$ and $\widetilde{A}_{rC}\setminus A_{rC}$.

The displacements $\underline{u}_w$ and $\underline{u}_r$ will be evaluated in the following through the numerical solution of Eq. (3). The knowledge of these unknown quantities will allow to calculate all the other required outputs like the contact areas $A_{wC}$ and $A_{rC}$ and the stresses $\sigma_w$ and $\sigma_r$. The contact forces $\underline{F}_{wC}$ and $\underline{F}_{rC}$ will be estimated by integration:

$$\underline{F}_{wC} = \int_{\widetilde{A}_{wC}}\underline{p}_w dA \quad \underline{F}_{rC} = \int_{\widetilde{A}_{rC}}\underline{p}_r dA. \quad (8)$$

### 5.4 The discretization of the model

Both the elastic bodies have been discretized by means of tetrahedral elements and linear shape functions. The meshes have been built according to the standard Delaunay's algorithms (see Fig. (8)). [16]

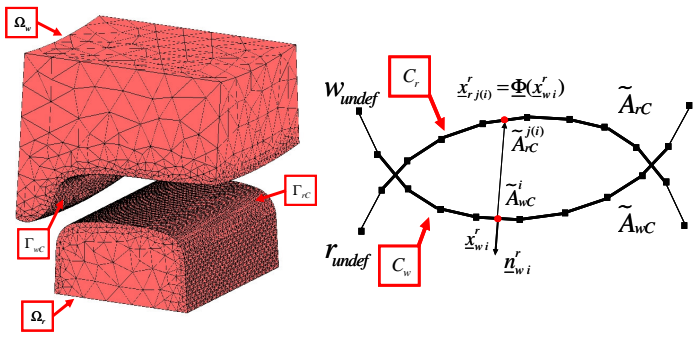


Figure 8: Discretization of the contact model.

The resolution of the meshes on the surfaces $\Gamma_{wC}$ and $\Gamma_{rC}$ is constant (usually in the range $1\text{mm} \div 2\text{mm}$) because the position and the dimensions of the contact patch are a priori unknown.
The surface resolution has also to assure an accuracy enough to correctly describe the contact phenomena. Moreover it is important to remark that the meshes have been created directly in the reference systems $O_{lw}x_{lw}y_{lw}z_{lw}$ and $O_{lr}x_{lr}y_{lr}z_{lr}$; therefore they don't change during the simulation and can be easily built off – line.
In the future the following convention will be adopted:
- the sets of all the elements of wheel and rail will be called $T_w$ and $T_r$ while the vectors $\underline{u}_{w\,h}, \underline{u}_{r\,l} \in R^{12}$ will contain the displacements of the four nodes belonging to the elements $h \in T_w$ and $l \in T_r$. Finally the vectors $\underline{U}_w$ and $\underline{U}_r$ will comprise the displacements relative to all the nodes of wheel and rail. Since the displacements on $\Gamma_{wD}$ and $\Gamma_{rD}$ are zero, the dimension of $\underline{U}_w$, $\underline{U}_r$ are $3(N_w - N_{wD})$ and $3(N_r - N_{rD})$, where $N_w$ and $N_r$ are the numbers of nodes of wheel and rail while $N_{wD}$ and $N_{rD}$ are the numbers of nodes on $\Gamma_{wD}$ and $\Gamma_{rD}$.
- similarly $C_w$ and $C_r$ will be the sets of the active contact elements on wheel and on rail, i. e. the sets of the elements having respectively a face $\widetilde{A}^i_{wC}$ and $\widetilde{A}^j_{rC}$ that lies on $\widetilde{A}_{wC}$ and $\widetilde{A}_{rC}$. The vectors $\underline{u}_{w\,i}, \underline{u}_{r\,j} \in R^{12}$ will contain the displacements of the four nodes belonging to the elements $i \in C_w$ and $j \in C_r$ while the vectors $\underline{U}_{wC}$ and $\underline{U}_{rC}$ will comprise the displacements relative to all the active elements. The dimension of $\underline{U}_{wC}$, $\underline{U}_{rC}$ are $3N_{wC}$ and $3N_{rC}$ where $N_{wC}$ and $N_{rC}$ are the number of nodes belonging to the active elements.
The knowledge of the relative kinematics ($\underline{O}^r_w$, $\dot{\underline{O}}^r_w$, $R^r_w$ and $\underline{\omega}^r_w$) and consequently of the estimated contact areas $\widetilde{A}_{wC}$ and $\widetilde{A}_{rC}$ allows to determine the sets $C_w$ and $C_r$ of the active contact elements on the wheel and on the rail.
For each active contact element on the wheel, the center $\underline{x}^r_{w\,i}$ of the face $\widetilde{A}^i_{wC}$ is considered. The normal projection $\underline{x}_{r\,j} = \underline{\Phi}(\underline{x}^r_{w\,i})$ of $\underline{x}^r_{w\,i}$ on $\widetilde{A}_{rC}$ will belong to the external face $\widetilde{A}^j_{rC}$ of the $j$-th active contact element on the rail. In particular the index $j(i)$ will be a function of the index $i$. In other words the pairs of points ( $\underline{x}^r_{w\,i}$ , $\underline{x}_{r\,j(i)}$ ) with $i \in C_w$ can be thought of as the discretization of the contact map $\underline{\Phi}$. The situation is schematically sketched in Fig. (8).
The values of the displacements $\underline{u}^r_w$, $\underline{u}_r$ and of their Jacobians $J^r_w$, $J_r$ in the points $\underline{x}^r_{w\,i}$ and $\underline{x}_{r\,j}$ are evaluated through the shape functions. [10] [11] [16]
At this point the distance function $d_i = d(\underline{x}^r_{w\,i})$ and the pressure $\underline{p}^r_{w\,i} = \underline{p}^r_w(\underline{x}^r_{w\,i})$ on the face $\widetilde{A}^i_{wC}$ of the active element of the wheel can be calculated by means of Eq. (1), (4) and (6). Finally a discrete version of the action – reaction principle (the Newton's Third Law) is needed to evaluate the pressure $\underline{p}_{r\,j} = \underline{p}_r(\underline{x}_{r\,j})$ on the face $\widetilde{A}^j_{rC}$ of the active element of the rail:

$$|\widetilde{A}^j_{rC}|\,\underline{p}_{r\,j} = |\widetilde{A}^i_{wC}|\,\underline{p}^r_{w\,i} \tag{9}$$

where $|\widetilde{A}^i_{wC}|$ and $|\widetilde{A}^j_{rC}|$ are the areas of the faces $\widetilde{A}^i_{wC}$ and $\widetilde{A}^j_{rC}$. Both the pressures $\underline{p}^r_{w\,i}$ and $\underline{p}_{r\,j}$ are supposed to be constant on $\widetilde{A}^i_{wC}$ and $\widetilde{A}^j_{rC}$.
The standard FEM techniques allow to discretize the weak form of the contact problem (see Eq. (3)) : [10] [11] [16]

$$\begin{aligned}
&\int_{\Omega_w} \sigma_w(\underline{u}_w) : \varepsilon_w(\underline{v}_w)\, dV = \sum_{h \in T_w} \underline{u}^T_{w\,h} K_{w\,h} \underline{v}_{w\,h} = \underline{U}^T_w K_w \underline{V}_w \\
&\int_{\Omega_r} \sigma_r(\underline{u}_r) : \varepsilon_r(\underline{v}_r)\, dV = \sum_{l \in T_r} \underline{u}^T_{r\,l} K_{r\,l} \underline{v}_{r\,l} = \underline{U}^T_r K_r \underline{V}_r \\
&\int_{\widetilde{A}_{wC}} \underline{p}_w \bullet \underline{v}_w\, dA = \sum_{i \in C_w} \underline{p}^T_{w\,i} M_{w\,i} \underline{v}_{w\,i} = \underline{F}_w(\underline{U}_{wC}, \underline{U}_{rC})^T \underline{V}_w \\
&\int_{\widetilde{A}_{rC}} \underline{p}_r \bullet \underline{v}_r\, dA = \sum_{i \in C_w} \underline{p}^T_{r\,j(i)} M_{r\,j(i)} \underline{v}_{r\,j(i)} = \underline{F}_r(\underline{U}_{wC}, \underline{U}_{rC})^T \underline{V}_r
\end{aligned} \tag{10}$$

where $K_{w\,h}$, $K_{r\,l}$ are the stiffness matrices relative to the elements $h \in T_w$, $l \in T_r$ and $M_{w\,i}$, $M_{r\,j}$ depend on the shape functions. The global stiffness matrices $K_w$ and $K_r$ are symmetric, positive defined and sparse while the vectors $\underline{F}_w$ and $\underline{F}_r$, that contain the terms due to the contact pressures, are sparse. Moreover the global stiffness matrices are evaluated directly in the reference systems $O_{lw}x_{lw}y_{lw}z_{lw}$ and $O_{lr}x_{lr}y_{lr}z_{lr}$; therefore they don't change during the simulation and can be easily built off – line. Eq. (3) and Eq. (10), combined together, give

$$\begin{aligned}
&\underline{U}^T_w K_w \underline{V}_w = \underline{F}_w(\underline{U}_{wC}, \underline{U}_{rC})^T \underline{V}_w \quad \forall \underline{V}_w \in R^{3(N_w - N_{wD})} \\
&\underline{U}^T_r K_r \underline{V}_r = \underline{F}_r(\underline{U}_{wC}, \underline{U}_{rC})^T \underline{V}_r \quad \forall \underline{V}_r \in R^{3(N_r - N_{rD})}
\end{aligned} \tag{11}$$

Finally, since the matrices $K_w$, $K_r$ are symmetric and the vectors $\underline{V}_w$, $\underline{V}_r$ are arbitrary, the following nonlinear system of algebraic equations is obtained:

$$K_w \underline{U}_w = \underline{F}_w(\underline{U}_{wC}, \underline{U}_{rC}) \quad K_r \underline{U}_r = \underline{F}_r(\underline{U}_{wC}, \underline{U}_{rC}) \tag{12}$$

where, as said before, the contact displacements $\underline{U}_{wC}$, $\underline{U}_{rC}$ are a subset of the displacements $\underline{U}_w$, $\underline{U}_r$. Eq. (12) can be also written as

$$\underline{U}_w = H_w \underline{F}_w(\underline{U}_{wC}, \underline{U}_{rC}) \quad \underline{U}_r = H_w \underline{F}_r(\underline{U}_{wC}, \underline{U}_{rC}) \qquad (13)$$

where the matrices $H_w = K_w^{-1}$ and $H_r = K_r^{-1}$ are symmetric, positive defined and full (consequently their storage can require an high memory consumption). Like $K_w$ and $K_r$ they don't change during the simulation and can be calculated off – line. Splitting $\underline{U}_w$, $\underline{U}_r$ into contact displacement $\underline{U}_{wC}$, $\underline{U}_{rC}$ and non – contact displacement $\underline{U}_{wNC}$, $\underline{U}_{wNC}$, Eq. (13) becomes

$$\begin{pmatrix} \underline{U}_{wNC} \\ \underline{U}_{wC} \end{pmatrix} = \begin{bmatrix} H_w^{11} & H_w^{12} \\ H_w^{21} & H_w^{22} \end{bmatrix} \begin{pmatrix} \underline{0} \\ \underline{f}_w(\underline{U}_{wC}, \underline{U}_{rC}) \end{pmatrix}$$
$$\begin{pmatrix} \underline{U}_{rNC} \\ \underline{U}_{rC} \end{pmatrix} = \begin{bmatrix} H_r^{11} & H_r^{12} \\ H_r^{21} & H_r^{22} \end{bmatrix} \begin{pmatrix} \underline{0} \\ \underline{f}_r(\underline{U}_{wC}, \underline{U}_{rC}) \end{pmatrix} \qquad (14)$$

In this way the second and the fourth components of Eq. (14) are sufficient to calculate contact displacement $\underline{U}_{wC}$, $\underline{U}_{rC}$:

$$\underline{U}_{wC} = H_w^{22} \underline{f}_w(\underline{U}_{wC}, \underline{U}_{rC}) \quad \underline{U}_{rC} = H_r^{22} \underline{f}_r(\underline{U}_{wC}, \underline{U}_{rC}) \cdot \qquad (15)$$

The matrices $H_w^{22}$ and $H_r^{22}$ have the same properties as $H_w$ and $H_r$ but this time their dimensions are much smaller. However $H_w^{22}$ and $H_r^{22}$ change during the simulation and therefore have to be built directly on – line. The vectors $\underline{f}_w$ and $\underline{f}_r$ are full. The remaining non – contact displacements $\underline{U}_{wNC}$, $\underline{U}_{wNC}$ can be evaluated by means of the first and the third components of Eq. (14).

The knowledge of the displacements $\underline{U}_w$, $\underline{U}_r$, evaluated by solving Eq. (12) or Eq. (15), allows to calculate all the other required outputs like the contact areas $A_{wC}$ and $A_{rC}$ and the stresses $\sigma_w$ and $\sigma_r$. The contact forces $\underline{F}_{wC}$ and $\underline{F}_{rC}$ are estimated by numerical integration:

$$\underline{F}_{wC} = \sum_{i \in C_w} | \tilde{A}_{wC}^i | \underline{p}_{w\,i} \quad \underline{F}_{rC} = \sum_{j \in C_r} | \tilde{A}_{rC}^j | \underline{p}_{r\,j} \cdot \qquad (16)$$

### 5.5 The numerical solution of the discrete problem

In this paragraph the numerical methods used for solving the discrete contact problem (15) are presented. Eq. (15) is a full non linear system with small dimensions. In particular, the typical dimensions of $H_w^{22}$ and $H_r^{22}$ (depending on the number of active elements) are about $100 \div 1000$.

Due to the small dimension of the problem, a Newton-LU method has been implemented in order to solve system (15).[21] Newton-LU is a Newton-type method for the problem $\underline{F}(\underline{x}) = \underline{0}$ where $\underline{F}$ is a generic nonlinear function. In particular, in this procedure, the Gauss method is employed to solve the arising linear systems:

$$F'(\underline{x}_k)\underline{s}_k = -\underline{F}(\underline{x}_k) \qquad (17)$$

where $F'(\underline{x})$ is the Jacobian matrix of $\underline{F}(\underline{x})$ and $\underline{s}_k$ is the Newton step. It has to be remarked that this approach needs the computation and the storage of the whole Jacobian at each iteration. Therefore, this procedure may be very expensive in terms of time consuming even though the small dimension.

In order to reduce the computational load, also a strategy based on a Newton-Krylov method (implemented in "matrix free" way) has been considered. [18] [23] Newton-Krylov methods are Newton-type methods where a Krylov method is employed to solve approximately the arising linear systems (17).

The Krylov method computes, at each iteration, the so-called inexact Newton step $\tilde{\underline{s}}_k$ which satisfies the condition:

$$\left\| \underline{F}'(\underline{x}_k)\tilde{\underline{s}}_k + \underline{F}(\underline{x}_k) \right\| \le \eta_k \left\| \underline{F}(\underline{x}_k) \right\| \qquad (18)$$

where the forcing terms $\eta_k \in [0,1)$ are used to control the level of accuracy. [18] As regards the considered problem, numerical experimentations showed that, among all the Krylov methods, the best iterative linear solver is the BiCGStab. [19] This kind of numerical procedures are known as Newton –BiCGStab methods.

An interesting feature of Newton – BiCGStab methods is that they require only the action of $F'(\underline{x})$ on a vector $\underline{v}$ but not the computation and the storage of the whole Jacobian. In this case, the product $F'(\underline{x})v$ can be approximated by finite differences [20]:

$$F'(\underline{x})\underline{v} \simeq \frac{\underline{F}(\underline{x} + \varepsilon \underline{v}) - \underline{F}(\underline{x})}{\varepsilon} \qquad (19)$$

where $\varepsilon > 0$ is a scalar small enough. Consequently these methods are called "matrix free".

It has been observed that a small number of nonlinear iterations is needed for solving the nonlinear system (15) and that the convergence is achieved in almost all cases. Consequently the choice of a less accurate solution of the Newton equations (17) turned out to be very efficient and effective in reducing the norm of $\underline{F}$. A constant forcing term $\eta_k = \eta \le 0.5 \ \forall k$ has been chosen.

Moreover, it has to be remarked that, if the guarantee of convergence is only local, both the numerical procedures presented may fail in finding a solution, even though an effective solution exists. Therefore Newton – LU and Newton – BiCGStab methods have been embedded into a globalization strategy. A monotone line search method with Armijo rule has been employed, with a maximum of 10 backtracks for nonlinear iteration. [20] [21]

Both the methods stop if the following stopping criterion is satisfied:

$$\|\underline{F}(\underline{x})\| < Tol \cdot \qquad (20)$$

The comparison between the performances of the different strategies will be reported in following chapter.
As regards the time integration of the whole model (multibody model and contact model; see Fig. (2)), explicit ODE solvers with variable step and variable order have been considered. [22] Moreover, during the simulations, the initial conditions for the nonlinear solvers (i.e. the Newton – BiCGStab and Newton – LU methods) are continually updated in order to speed up the convergence of the solvers and to reduce the computation time. In other words the solution of the problem at the current time step is used as initial condition for the solver at the next time step.

## 6 NUMERICAL SIMULATION

In order to study the behavior of the whole model, a large number of simulations has been carried out on many different railway tracks. The performances of the model have been evaluated both in terms of output accuracy (kinematic variables, contact forces and contact patch) and in terms of numerical efficiency (performances of the numerical algorithms and time consumption).

### 6.1 Performances of the numerical methods

In this section the performances of the numerical procedures described in paragraph 5.5 will be analyzed and compared to each other. To this purpose a typical simulation of the lateral dynamics of the Manchester Wagon has been considered. [5] [15] The simulations have been performed on a curvilinear railway track, the data of which are reported in Tab. (3).
The comparison between the numerical methods has been carried out on a machine equipped with an Intel Xeon 2.66GHz, 8GB RAM using Matlab R2007b (machine precision $\varepsilon_m = 2*10^{-16}$).
In order to establish the best ODE solver, several experimentations have been performed with the ODE23 and the ODE45. [22] The value of the main numerical parameters are reported in Tab. (4).

RelTol and AbsTol are the relative and absolute tolerances of the ODE solvers, MaxitNonlin, MaxitLin are the maximum number of nonlinear and linear iterations, Tol is the stopping tolerance and $\eta$ is the forcing term. In particular the value of the stopping tolerance Tol has been chosen to assure a sufficient accuracy (in terms of displacements and contact pressures) and, at the same time, to minimize the computation time.
Tab. (5) summarizes the results obtained by using the ODE 23 and the ODE 45. For each wheel – rail contact pair (Right and Left) the following data have been considered:

| | | |
|---|---|---|
| Curvature | $K$ | 1/1200 m$^{-1}$ |
| Slope | $p$ | 0 |
| Cant | $\beta$ | 60 mm |
| Laying angle | $\alpha_p$ | 1/40 rad |
| Velocity | $V$ | 45 m/s |
| Friction coefficient | $\mu$ | 0.3 |

Table 3: Data of the railway track

| | |
|---|---|
| Differential Contact Model | Eq. (15) |
| RelTol / AbsTol | $10^{-8}$ / $10^{-6}$ |
| Nonlinear Solver | Newton - BiCGStab |
| Tol / MaxitNonlin | $10^{-8}$ / 20 |
| $\eta$ / MaxitLin | 0.01 / 20 |

Table 4: Numerical parameters.

the number #cps of contact problem solved (equal for both the contact pairs), the total number #New of nonlinear iterations, the average number #BiCGS of linear iterations for each nonlinear iteration and the total computation time.

| ODE23 - Newton-BiCGStab | | | | |
|---|---|---|---|---|
| | #cps | #New | #BiCGS | time |
| R | 31814 | 27409 | 2.9 | 8396 sec (~2h 20min) |
| L | | 29495 | 3.5 | |
| **ODE45 - Newton-BiCGStab** | | | | |
| | #cps | #New | #BiCGS | time |
| R | 45710 | 44625 | 3.1 | 12870 sec (~3h 34min) |
| L | | 46170 | 3.5 | |

Table 5: Comparison between ODE23 and ODE45.

The results show that low order solvers like the ODE23 turn out to be better than high order solvers like ODE45.
As said in the paragraph 5.5, Eq. (15) can be also solved by means of a Newton – LU strategy. Tab (6) contains the results obtained by solving (15) with this approach. The used ODE solver is the ODE23, while the other numerical parameters are the same reported in Tab. (4).

| ODE23 - Newton-LU | | | |
|---|---|---|---|
| | #cps | #New | time |
| R | 30401 | 23936 | 39096 sec (~10h 51min) |
| L | | 24306 | |

Table 6: Newton – LU for solving Eq.(15).

Looking at Tab. (6), the Newton – BiCGStab methods (matrix free) are more efficient than the Newton – LU methods. In particular the computation and the storage of the Jacobian matrix at each nonlinear iteration turned out to be too time-consuming.
Finally, in order to justify the choice of the constant forcing term $\eta = 10^{-2}$, some experimentations have been performed by using the following values of the parameter: $\eta = 0.5,\ 10^{-1},\ 10^{-2},\ 10^{-3},\ 10^{-4}$. As usual the employed ODE solver is always the ODE23. The results have been reported in terms of computation time (see Fig.(9)).

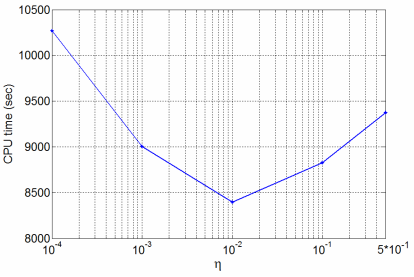


Figure 9: Computation time as a function of the forcing term $\eta$

### 6.2 The SIMPACK RAIL 2D multibody model

The same multibody model of the benchmark vehicle (the Manchester Wagon [14]) has been implemented also in Simpack Rail, a widely tested and validated multibody software for the analysis of the railway vehicle dynamics. This time the multibody model is equipped with a standard contact model based on the semi – elastic approach. [4] [5] [6] As in the previous case the 2D multibody model (designed for the study of the lateral dynamics) has been obtained from the fully 3D multibody model of the vehicle while the contact model is completely 3D (see Fig. (10)). The comparison between the results obtained by the Matlab/Simulink model and those obtained by the Simpack Rail model has allowed an accurate and reliable validation of the new contact model.

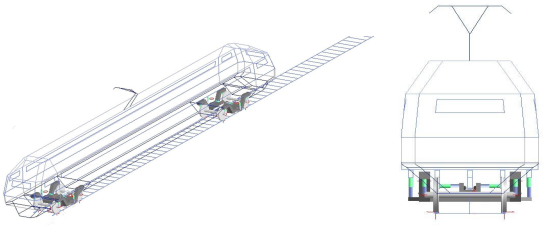

Figure 10: 3D and 2D multibody models of the Manchester Wagon (Simpack Rail).

### 6.3 Simulation of the lateral vehicle dynamics

The comparison between the Matlab/Simulink model (implemented on Matlab R2007b) and the Simpack Rail model (implemented on Simpack 8.900) has been carried out on the same curvilinear railway track introduced above (see Tab. (3)). [5] [15] The numerical data relative to the Matlab model have been chosen starting from the results obtained in the paragraph 6.1 (See Tab. (4)). The used ODE solver is ODE23. Similarly the numerical data relative to the Simpack model are briefly summarized in Tab. (7).

| | |
|---|---|
| ODE Solver | ODE 5 (Dormand - Prince) |
| Fixed Step | $5*10^{-4}$ |
| Contact Model | Semi – Elastic Approach |

Table 7: Numerical Data (Simpack model).

Among all the kinematic and dynamic variables evaluated by the models, the time histories of the following quantities are reported (for the sake of simplicity all the outputs are expressed in the reference system $O_R x_R y_R z_R$):

- the lateral displacement $y_W^R$ of the centre of mass of the wheelset $\underline{O}_W^R$ (Fig. (11))
- the lateral displacement $y_B^R$ of the centre of mass of the body – car $\underline{O}_B^R$ (Fig. (12))
- the contact forces on the left wheel $\underline{F}_{lw}^R$ and on the right wheel $\underline{F}_{rw}^R$; in particular $Y_{lw}^R$ and $Y_{rw}^R$ are the lateral forces (Fig. (13) and Fig. (15)) while $Q_{lw}^R$ and $Q_{rw}^R$ are the vertical forces (Fig. (14) and Fig. (16)).

The Matlab variables are plotted in blue while the equivalent Simpack quantities in red.

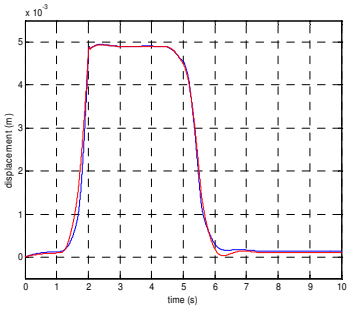


Figure 11: Lateral displacement $y_W^R$

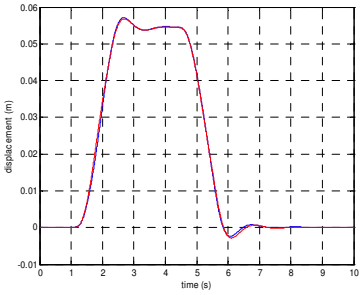


Figure 12: Lateral displacement $y_B^R$

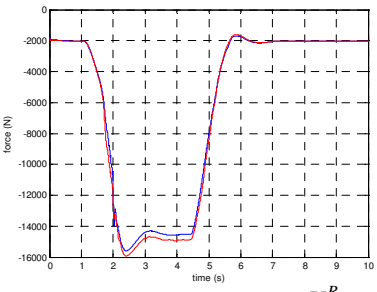


Figure 13: Lateral force $Y_{lw}^R$

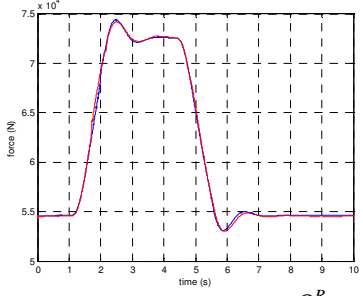


Figure 14: Vertical force $Q_{lw}^R$

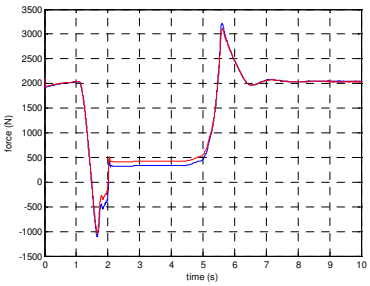


Figure 15: Lateral force $Y_{rw}^R$

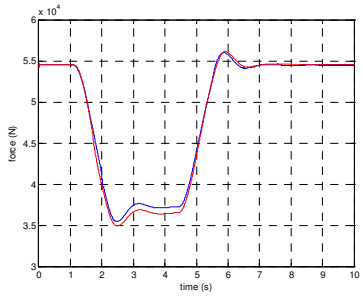


Figure 16: Vertical force $Q_{rw}^R$

The simulation results show a good agreement between the Matlab model and the Simpack model both in terms of kinematic variables and in terms of contact forces.

As regards the positions of contact patches $A_{wC}$, $A_{rC}$ on the wheel and on the rail, in order to give an effective description of the shifting of the contact areas during the simulation, a lateral section along the plane $y_R z_R$ of the areas $A_{wC}$, $A_{rC}$ has been considered. Moreover the sections of the contact patches have been plotted on cylindrical surfaces generated by the wheel and rail profiles and as long as the distance traveled by the vehicle. By convention $A_{lwC}$, $A_{rwC}$ are the contact areas on the left and on the right wheel (Fig. (17) and Fig. (18)) while $A_{lrC}$, $A_{rrC}$ are the contact areas on the left and on the right rail (Fig. (19) and Fig. (20)).

The sections of the contact areas evaluated by the Matlab model are plotted in blue while the contact points detected by the Simpack model are plotted in black. It is interesting to remark that, during the curve, a second contact point appears on the left wheel and rail (the track turns to left). Consequently, while the Simpack model detects two distinct contact points, the contact areas evaluated by the Matlab model consist of two disjoint parts. Also in this case the agreement

between the results obtained by the Matlab model and the Simpack model is good.
In conclusion the accuracy of the Matlab model turns out to be comparable with that of the Simpack model; moreover the quasi – total absence of numerical noise highlights the robustness and the stability of the new differential contact model.

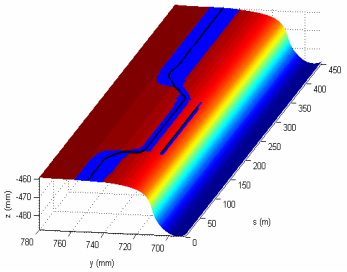


Figure 17: Section of contact area $A_{lwC}$

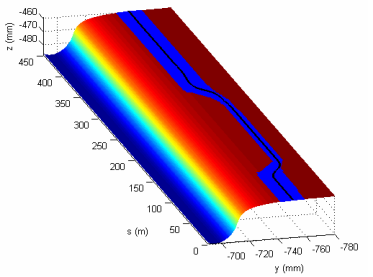


Figure 18: Section of contact area $A_{rwC}$

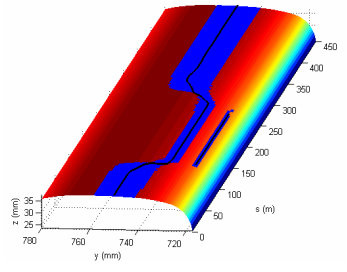


Figure 19: Section of contact area $A_{lrC}$

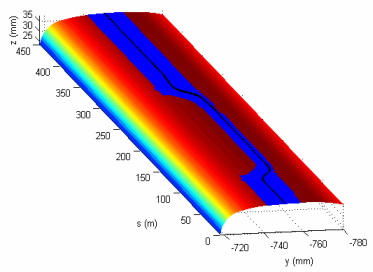


Figure 20: Section of contact area $A_{rrC}$

## 7 CONCLUSION AND PERSPECTIVE

The performances of the Matlab model turned out to be good both in terms of output accuracy (kinematic variables, contact forces and contact patch) and in terms of numerical efficiency (performances of the numerical algorithms and time consumption) and satisfy all the specifics reported in the introduction (see chapter 1).
As regards the further developments, in the near future fully 3D multibody models of the Manchester Wagon will be considered. This kind of model allows a complete description of the vehicle dynamics but obviously involves an increase of the model DOFs and of the number of wheel – rail contact pairs. Moreover many optimizations of the differential contact model are planned for the future. The improvements will regard especially the FEM techniques used to discretize the contact problem. In particular new mesh generation algorithms and suitable nonlinear shape functions will be examined. These techniques assure a better accuracy in the description of the local contact phenomena but increases the dimension of the discrete problem and consequently the computational load and the memory consumption. Finally the implementation of the contact model in programming environments like C/C++ and FORTRAN will be considered in order to obtain a further reduction of the computation time.

## REFERENCES


[1] A. A. Shabana and J. R. Sany: *Nonlinear Dynamics*, 2001, vol. 24, pp 183 – 204.

[2] S. Iwinicki: *Fatigue and Fracture of Engineering Materials and Structures*, 2003, vol. 26, pp 887 – 900.

[3] J. Pombo and J. Ambrosio: *International Journal of Vehicle Systems Modelling and Testing*, 2005, vol. 1, pp 79 – 105.

[4] J. J. Kalker: *Three – dimensional Elastic Bodies in Rolling Contact*, Kluwer Academic Publishers, Dordrecht, Netherlands, 1990.

[5] R. V. Dukkipati and J. R. Amyot: *Computer Aided Simulation in Railway Dynamics*, Dekker, New York, 1988.

[6] O. Polach: *Wear*, 2005, vol. 258, pp 992 – 1000.

[7] A. A. Shabana, K. E. Zaazaa, J. L. Escalona and J. L. Sany: *Journal of Sound and Vibration*, 2004, vol. 269, pp 295 – 325.

[8] S. Falomi, M. Malvezzi, E. Meli and A. Rindi: *Multibody System Dynamics*, 2008, vol. 20(4), pp 327 – 358.

[9] K. L. Johnson: *Contact Mechanics*, Cambridge University Press, Cambridge, England, 1985

[10] N. Kikuchi and J. T. Oden: *Contact Problems in Elasticity*, SIAM Studies in Applied Mathematics, Philadelphia, Pennsylvania, 1988.

[11] P. Wriggers: *Computational Contact Mechanics*, John Wiley & Sons, Hoboken, New Jersey, 2002.

[12] O. Zienkiewicz: *The Finite Element Method in Engineering Science*, McGraw – Hill, New York, 1988.

[13] A. Klarbring: *Computer Methods in Applied Mechanics and Engineering*, 1986, vol. 58, pp 175 – 200.

[14] S. Iwinicki: *The Manchester Benchmarks for Rail Vehicle Simulators*, Swets & Zeitlinger, Lisse, Netherlands, 1999.

[15] C. Esveld: *Modern Railway Track,* Delft University of Technology, Delft, Netherlands, 2001.

[16] G. Dhatt and G. Touzot: *The Finite Element Method Displayed*, John Wiley & Sons, Hoboken, New Jersey, 1984.

[17] G. Vicuna: *Organizzazione e Tecnica Ferroviaria*, Ed. CIFI, Roma, Italy, 1986.

[18] R. S. Dembo, S. C. Eisenstat and T. Steihaug: *SIAM Journal of Numerical Analysis*, 1982, vol. 19, pp 400 – 408.

[19] C.T. Kelley: *Iterative Methods for Linear and Nonlinear Equations*, SIAM, Philadelphia, Pennsylvania, 1995.

[20] Y. Saad: *Iterative Methods for Sparse Linear Systems*, SIAM, Philadelphia, Pennsylvania, 2003.

[21] J. Nocedal and S.J. Wright: *Numerical Optimization*, Springer Series in Operation Research, Berlin, Germany, 1999.

[22] L. F. Shampine and M. W. Reichelt: The MATLAB ODE Suite. *SIAM Journal on Scientific Computing*, 1997, vol. 18, pp 1 – 22.

[23] S. Bellavia and B. Morini: *SIAM Journal on Scientific Computing*, 2001, vol. 23, pp 940 – 960.